Earth's Energy Imbalance

KEVIN E. TRENBERTH AND JOHN T. FASULLO

National Center for Atmospheric Research,* Boulder, Colorado

MAGDALENA A. BALMASEDA

European Centre for Medium-Range Weather Forecasts, Shinfield Park, Reading, United Kingdom

ABSTRACT

Climate change from increased greenhouse gases arises from a global energy imbalance at the top of the atmosphere (TOA). TOA measurements of radiation from space can track changes over time but lack absolute accuracy. An inventory of energy storage changes shows that over 90% of the imbalance is manifested as a rise in ocean heat content (OHC). Data from the Ocean Reanalysis System, version 4 (ORAS4), and other OHC-estimated rates of change are used to compare with model-based estimates of TOA energy imbalance [from the Community Climate System Model, version 4 (CCSM4)] and with TOA satellite measurements for the year 2000 onward. Most ocean-only OHC analyses extend to only 700-m depth, have large discrepancies among the rates of change of OHC, and do not resolve interannual variability adequately to capture ENSO and volcanic eruption effects, all aspects that are improved with assimilation of multivariate data. ORAS4 rates of change of OHC quantitatively agree with the radiative forcing estimates of impacts of the three major volcanic eruptions since 1960 (Mt. Agung, 1963; El Chichón, 1982; and Mt. Pinatubo, 1991). The natural variability of the energy imbalance is substantial from month to month, associated with cloud and weather variations, and interannually mainly associated with ENSO, while the sun affects 15% of the climate change signal on decadal time scales. All estimates (OHC and TOA) show that over the past decade the energy imbalance ranges between about 0.5 and $1\,\mathrm{W\,m^{-2}}$. By using the full-depth ocean, there is a better overall accounting for energy, but discrepancies remain at interannual time scales between OHC- and TOA-based estimates, notably in 2008/09.

1. Introduction

With increasing greenhouse gases in the atmosphere, there is an imbalance in energy flows in and out of the earth system at the top of the atmosphere (TOA): the greenhouse gases increasingly trap more radiation and hence create warming (Solomon et al. 2007; Trenberth et al. 2009). "Warming" really means heating and extra energy, and hence it can be manifested in many ways. Rising surface temperatures are just one manifestation.

Melting Arctic sea ice is another. Increasing the water cycle and altering storms is yet another way that the overall energy imbalance can be perturbed by changing clouds and albedo. However, most of the excess energy goes into the ocean (Bindoff et al. 2007; Trenberth 2009). Can we monitor the energy imbalance with direct measurements, and can we track where the energy goes? Certainly we need to be able to answer these questions if we are to properly track how climate change is manifested and quantify implications for the future.

Therefore, key issues for Earth from an overall energy standpoint are the actual energy imbalance at the TOA and surface and their changes over time. Many other scientific problems of interest relate to the storage and movement of energy, including the exchanges among the climate system components (atmosphere, ocean, land, and cryosphere) and the changes in phase state, especially of water involving latent energy (ice, liquid, and vapor). Tracking how much extra energy has gone back to space (Murphy et al. 2009) and where this energy

has accumulated is possible, apparently with reasonable closure for 1993–2003 (Bindoff et al. 2007; Trenberth 2009), but has been problematic in recent years (Trenberth and Fasullo 2010). Over the past 50 years, the oceans have absorbed about 90% of the total heat added to the climate system while the rest goes to melting sea and land ice, warming the land surface and warming and moistening the atmosphere. Because carbon dioxide and other greenhouse gas concentrations have further increased since 2003, increasing radiative forcing to the tune of about $0.3\,W\,m^{-2}\,decade^{-1}$ (Solomon et al. 2007), the amount of heat subsequently being accumulated should be even greater, assuming the other external radiative forcing and the climate response remain unaltered. However, it is offset somewhat between 2005 and 2010 by reduced solar irradiance during a low sunspot activity period (Trenberth 2009; see Fig. 2 presented later) and perhaps by changes in atmospheric aerosols and stratospheric water vapor (Solomon et al. 2010, 2011; Vernier et al. 2011). Moreover, natural variability, notably El Niño–Southern Oscillation (ENSO) and other influences also play a role. Here we explore the extent to which we can assess the actual energy imbalance and its changes over time.

Quantifying the absolute energy imbalance requires a level of accuracy not available from any direct measurements whether from satelliteborne instruments (e.g., Loeb et al. 2009) or others. It can be estimated from climate model simulations, which in turn require validation to provide confidence in their results, and the results also depend on the veracity of the specified climate forcings. It can also be estimated by an inventory of the rates of changes of energy stored in all components of the climate system, the most important of which is the ocean and thus changes in the ocean heat content (OHC).

The changes in TOA energy imbalance over time do not require accurate knowledge of the absolute values, but rather they require a consistent stable set of instrumental measurements with adequate precision. That is, they may be biased in some, perhaps unknown, way. While the planetary imbalance at TOA is too small to measure directly from satellite, instruments are far more stable than they are absolutely accurate with calibration stability $<0.3\,W\,m^{-2}\,decade^{-1}$ (95% confidence) (Loeb et al. 2009). Tracking relative changes in Earth's energy flows by measuring solar radiation in and infrared radiation out to space, and thus changes in the net radiation, seems to be at hand from the current spaceborne instruments called Clouds and the Earth's Radiant Energy System (CERES) (Wong et al. 2009). The changes of energy anomalies can be compared with other methods, including from the inventory method and model simulations, as reported here.

Historical subsurface ocean observations (see section 2) come from a sparse unevenly distributed set of mainly subsurface temperature data collected by a large, disparate, and changing mixture of instruments with diverse accuracies and biases. Expendable bathythermographs (XBTs) were the main source from the late 1960s to 2004, but because depth or pressure of observations were not measured, issues in drop rate and its corrections plague these data and attempts to correct them result in varied outcomes. By 2005 the ocean observing system had reached new capabilities, as some 3000 Argo floats populated the ocean for the first time to provide regular temperature soundings of up to the upper 2000 m, giving new confidence in the OHC assessment. Hence, in the ocean for OHC, the pre-Argo and post-Argo eras may not be compatible for inventory analysis in determining changes over time. Other observing systems in place can nominally measure the major storage and flux terms, but owing to errors and uncertainty, it remains a challenge to track anomalies with confidence (Trenberth 2009; Trenberth and Fasullo 2010). Indeed, discrepancies between perceived changes in OHC and total energy on Earth and the inferred changes from CERES measurements became a matter of concern and known as the "missing energy" problem (Trenberth and Fasullo 2010; Loeb et al. 2012).

The global energy imbalance, however, is not constant in time, owing to the complexity of various climate forcings and also because of natural variability. For instance, ENSO fluctuations cause changes in heat storage in the ocean and there is a mini global warming at the end of El Niño events, as heat comes out of the ocean and is eventually radiated to space (e.g., Trenberth et al. 2002). The main natural externally forced variations are those from volcanic eruptions, such as from Mt. Pinatubo in 1991 (Trenberth and Dai 2007). Church et al. (2005) attempted to determine the volcanic signal, defined by an early generation climate model, in the sea level and uncorrected OHC record. Even the modest changes in total solar irradiance (TSI) with the sunspot cycle have a signature in the TOA energy imbalance. Many OHC datasets do not resolve these adequately, but a new ocean reanalysis from the European Centre for Medium-Range Weather Forecasts (ECMWF) called the Ocean Reanalysis System, version 4 (ORAS4) (Balmaseda et al. 2013a,b), shows ENSO- and volcanic-related OHC variability and is explored in detail here. Ocean reanalyses also help overcome many of the difficulties with an inhomogeneous observing system through bias corrections, use of multiple variables in the context of dynamical constraints, and by improved gap filling in space and time.

Section 2 discusses the different sources of information on the global energy imbalance. These include climate
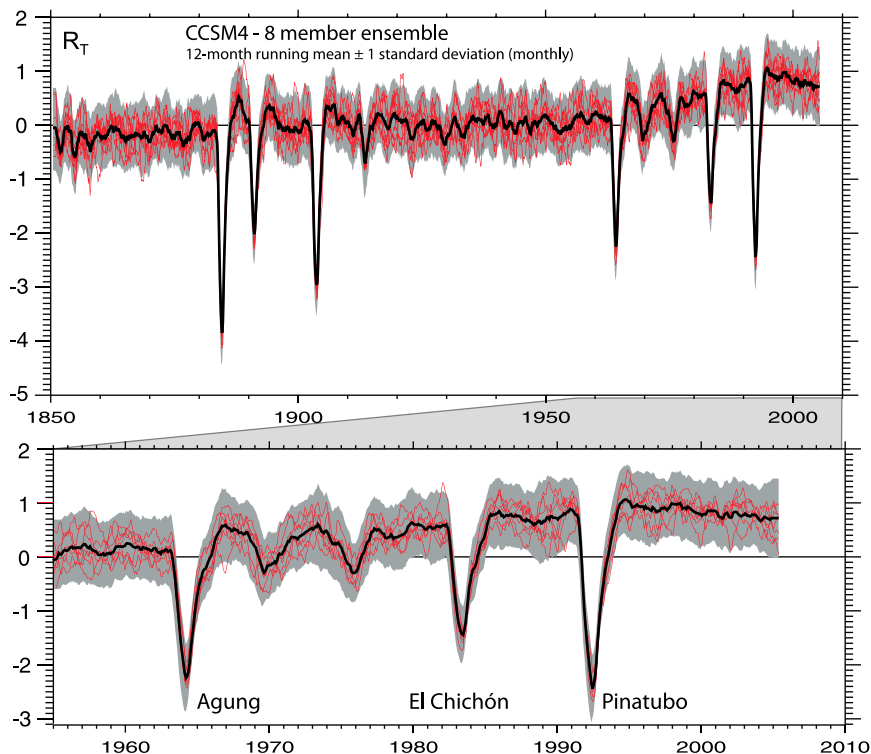
FIG. 1. (top) The net TOA radiation (down; $W\,m^{-2}$) from CCSM4 run at 1° resolution for eight members of the ensemble. Shown are the ensemble 12-month running mean (black line) with ± 1 standard deviation of the individual monthly values (gray shaded region) and the eight individual ensemble values as 12-month running means. (bottom) An expanded version of the last 50 years that includes the Mt. Agung, El Chichón, and Mt. Pinatubo volcanic eruptions.

model results and OHC-based estimates. It details strengths and issues with the OHC data, and especially in how to obtain rates of change of OHC. It then compares different estimates of OHC rates of change with the model-derived TOA values, quantifying the interannual variability and amplitude/timing of volcanoes. Section 3 presents the comparison for the last decade between OHC and CERES estimates of the imbalance. The conclusions are presented in section 4.

2. The global energy imbalance

a. Climate system energy inventory

Extensive use has been made of conservation of energy and the assumption that on a time scale of years, the change in heat storage within the atmosphere is very small (Trenberth et al. 2009). The net radiation at TOA R_T is the sum of the absorbed solar radiation (ASR) minus the outgoing longwave radiation (OLR): $R_T =$ ASR − OLR. In turn, the ASR is the difference between the incoming solar radiation and the reflected solar radiation.

Fasullo and Trenberth (2008a) provided an assessment of the global energy budgets at TOA and the surface, atmosphere, ocean, and land domains based on a synthesis of satellite retrievals, atmospheric reanalysis fields, a land surface simulation, and ocean temperature estimates. As well as Earth Radiation Budget Experiment (ERBE) data, they made use of the CERES measurements that became available part way through 2000 and assessed their differences. By exploiting both climate models and changes in OHC, Trenberth et al. (2009) deduced the imbalance to be $0.9\,W\,m^{-2}$ for the early 2000s, with 90% confidence limits of $\pm 0.5\,W\,m^{-2}$. Note that these estimates were made long before any of the results in Fig. 1 (presented below) were generated. Fasullo and Trenberth (2008b) evaluated meridional atmospheric energy transports for ocean, land, and global domains, while Trenberth and Fasullo (2008) provided an observationally based estimate of the mean and annual cycle of ocean energy divergence, and a comprehensive assessment of uncertainty. At that time, changes in OHC were the biggest source of errors. Trenberth et al. (2009) synthesized results into an updated global energy flow diagram and, to understand the
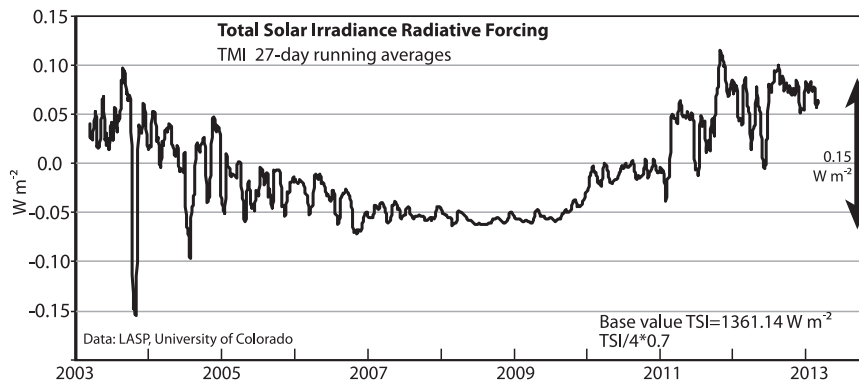
FIG. 2. Radiative forcing ($W\,m^{-2}$) from changes in total solar irradiance from the TIM instrument relative to a base value of TSI of $1361.14\,W\,m^{-2}$ as 27-day running averages. The double arrow at right shows the range of $0.15\,W\,m^{-2}$.

sources of error and the discrepancies among estimates, a breakdown of the budgets into land and ocean domains, and the annual and diurnal cycles, was considered.

Trenberth (2009) provided a more complete inventory of all the components of the climate system and changes in the sun, and their contributions to both global energy storage change and sea level rise. This included tracking the slight decrease in solar insolation from 2000 until 2009 with the ebbing 11-yr sunspot cycle (Trenberth 2009). While there was a reasonable accounting for the energy imbalance and sea level rise from 1993 to 2003, there was a shortfall in accounting for the energy imbalance in the more recent period from 2004 to 2008. This led to the concept of missing energy as detailed in Trenberth and Fasullo (2010). In particular, in 2008/09 CERES observations showed an increase in the TOA energy imbalance just at the time the surface temperatures and upper OHC were below averages over recent years, highlighting the question of "where did the energy go?" Several more recent studies have weighed in on this issue, as discussed below.

An observed change of $5{-}12 \times 10^{22}\,J\,decade^{-1}$ in OHC in the 2000s (section 2c; Fig. 4) corresponds to 0.3–0.75 $W\,m^{-2}$ global heating, and this can be compared with estimates of the amount of heat taken, in units of $10^{21}\,J\,decade^{-1}$, to (i) melt Arctic sea ice (1 unit); (ii) melt ice sheets of Greenland and Antarctica (1.5 units); (iii) melt total land ice (2–3 units); (iv) warm land (2 units); and (v) warm and moisten the atmosphere (1 unit). Summing all of these and adding 1 to 2 for the rest of the sea ice gives 8 units compared with 50–120 for the ocean (based on Trenberth 2009). Hansen et al. (2011) assessed the nonocean components of the energy balance as about $0.07\,W\,m^{-2}$ in the 2002–07 period or about 11 units, with the main difference being a larger land contribution (4 units). Nonocean contributions were

much lower in earlier decades, averaging about $0.02\,W\,m^{-2}$ in the 1980s and $0.04\,W\,m^{-2}$ in the 1990s (Hansen et al. 2011). Accordingly, changes in OHC dominate.

b. Model results

To set the stage, Fig. 1 shows the results for R_T (down) from the National Center for Atmospheric Research (NCAR) Community Climate System Model, version 4 (CCSM4) (Gent et al. 2011), from eight ensemble members of runs for the past 155 years (1850–2005), with specified external forcings from changing atmospheric composition and the sun (Ammann et al. 2003). Included are natural variations from volcanic aerosols as well as increasing greenhouse gases and changing tropospheric aerosols from human activities. However, effects of minor volcanic eruptions after Mt. Pinatubo in 1991 (see Vernier et al. 2011) are not included. The total solar irradiance varies and fluctuates by a range of about $1\,W\,m^{-2}$ over recent sunspot cycles. To convert these variations into radiative forcing requires dividing by the ratio of the cross section area (πa^2, where a is the Earth's radius) to the area of the surface ($4\pi a^2$) and thus a factor of 4 and allowing for the 30% or so reflected. Radiative forcing fluctuations computed from the Total Irradiance Monitor (TIM) (University of Colorado) measurements of TSI, with a 27-day running average (to accommodate the sun's rotation) and multiplied by 0.7/4 to allow for an approximate albedo effect (Fig. 2), show variations ranging over about $0.15\,W\,m^{-2}$.

The model replicates the global mean temperatures over this period (Fig. 1) reasonably well (not shown), although the trend is slightly larger than observed as there are no indirect effects of aerosols on clouds included (Gent et al. 2011). The eight ensemble members have modest variations from one to the other owing to natural variability. Standard deviations of monthly means

among the ensemble members (Fig. 1) average $0.62\,\mathrm{W\,m^{-2}}$ (averaged over all 156 years). However, Fig. 1 also shows the individual CCSM4 runs as 12-month running means, and these variations nearly all fit within the envelop of the 1-month standard deviations, with a standard deviation (of the 12-month running means) about the ensemble mean of $0.25\,\mathrm{W\,m^{-2}}$ and a reduction in monthly variance by a factor of 6.2. This suggests that a lot of monthly variability is random, with an autocorrelation time scale of only a few months, and is associated with weather noise and transient variations in clouds. The model monthly and interannual variability compares well with those of CERES (0.62 and $0.28\,\mathrm{W\,m^{-2}}$ for total and interannual, respectively, estimated for the period March 2000–June 2012), although the CERES inter- annual signal also includes variations in the forcing, such as from the changing TSI.

Nevertheless, there are strong variations over time associated with the external radiative forcings of the model. Of particular note are the sharp drops associated with volcanic eruptions, embedded within the overall positive trend after about the early 1960s rising to a consistent energy imbalance in the 2000s of about $0.9\,\mathrm{W\,m^{-2}}$. Variations among the ensemble members over decadal time scales (Fig. 1) are mostly within $\pm0.1\,\mathrm{W\,m^{-2}}$, of the same order as variations in solar forcing.

Figure 1 highlights the volcanic eruptions after 1960 in the lower panel: Mt. Agung (February–March 1963), El Chichón (March–April 1982), and Mt. Pinatubo (June 1991), as well as some more minor events. In CCSM4 the volcanic perturbations were based on the idealized re- constructions from Ammann et al. (2003), using esti- mates of the total amount of sulfate released by each eruption and a built-in consistent meridional spread and decay of volcanic aerosol at monthly resolution taking into account the seasonally changing stratospheric transport. The profile of aerosol forcing for the El Chichón eruption in the 1980s averaged at 18°N is shown in Fig. 3, and this can be compared with direct mea- surements of changes in solar radiation at Mauna Loa (e.g., Deluisi et al. 1983; Dutton and Bodhaine 2001), where the masking occurred very rapidly following the eruption. For El Chichón, the peak aerosol at 18°N in the CCSM4 runs was not until September, which is some 6 months after what actually occurred. As we show later (section 2d), this places the timing of CCSM radiative forcing at odds with changes in observed OHC for this eruption.

c. OHC

A compilation of annual values of OHC for the top 700 m of the ocean from several sources is given by Balmaseda et al. (2013a) and updated in Fig. 4. The
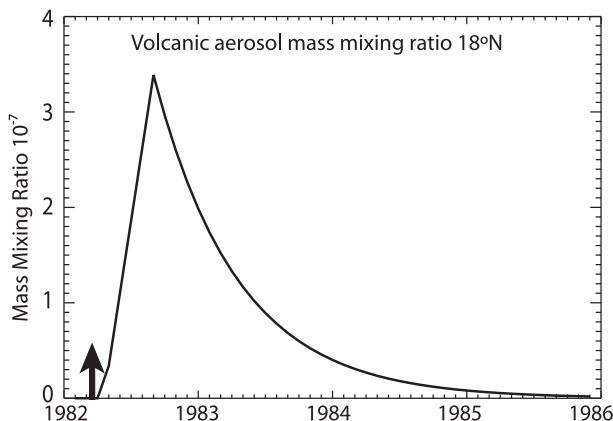

FIG. 3. The profile of aerosol mass mixing ratio in the strato- sphere for the El Chichón eruption in the 1980s averaged at 18°N from the CCSM4 run. The time of the eruption is given by the thick arrow and the subsequent evolution is specified in an idealized manner as to the meridional spread and time of peak and sub- sequent decay based on Ammann et al. (2003).

following introduces the many analyses and their find- ings, although a more thorough review is given in Abraham et al. (2013). The data and their corrections vary considerably, but in addition, analysis methods and periods also vary, so that there remain surprisingly large differences among the different estimates. The next subsection examines rates of change of OHC (also given in Fig. 6). Here we focus on the extent to which the re- sults seem useful and realistic, and we ask the question of whether the known climate forcings are reflected in the OHC results. The figures presented here place the findings in context.

Major corrections to XBTs since the Intergovernmental Panel on Climate Change Fourth Assessment Report (IPCC AR4) (Bindoff et al. 2007) removed a lot of spurious decadal variability in the record (Domingues et al. 2008; Ishii and Kimoto 2009; Levitus et al. 2009; Gouretski and Reseghetti 2010). Xue et al. (2012) compared OHC estimates for the top 300 m of the ocean, mainly compiled for operational monitoring purposes, and found shortcomings although with reduced un- certainty after 2005. Lyman et al. (2010) assessed various methods and datasets related to OHC changes over time for the top 700 m. They estimated average 1993–2008 heat gain as $0.64 \pm 0.11\,\mathrm{W\,m^{-2}}$, where the uncertainty range is the 90% confidence interval. According to Hansen et al. (2011), the Lyman et al. (2010) upper- ocean heat yields a planetary energy imbalance of $0.80\,\mathrm{W\,m^{-2}}$ when taking account of the other compo- nents of the climate system (deeper ocean, melting sea ice, glacial ice, etc.). Levitus et al. (2009) found smaller heat gains in the upper 700 m of $0.41\,\mathrm{W\,m^{-2}}$, yielding a planetary energy imbalance of only $0.57\,\mathrm{W\,m^{-2}}$, according
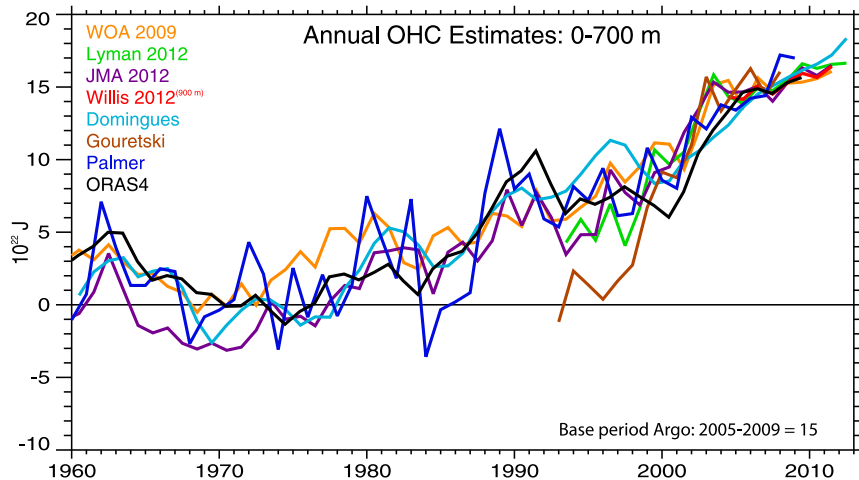
FIG. 4. Annual values of OHC to 700 m (900 m for Willis), except for Domingues, which is a 3-yr running mean. Here the common period for Argo of 2005–09 is set to a value of 15×10^{22} J.

to Hansen et al. (2011). Johnson et al. (2012) update the Lyman et al. (2010) values through 2011 and account for some quality control issues to find a linear warming rate of about 0.48 W m^{-2} for 1993–2011; however, they indicate a much sharper rate of increase in the Hadley Centre (Palmer et al. 2007) OHC from 2001 to 2005.

Figure 4 presents a compilation of the main available OHC from 0 to 700 m, referenced to the recent data rich Argo period of 2005–09, which is set to 15 × 10^{22} J. There are clear upward trends in upper OHC after 1970. Sampling uncertainties are reduced over time (Domingues et al. 2008), and 1σ standard error in OHC for the top 700 m in 10^{22} J ranges among 5.6 in 1960, 2.7 in 1970, 2.1 in 1980, 1.8 in 1990, 1.5 in 2000, and 1.4 in 2003. Lyman et al. (2010) estimate the total sources of error more thoroughly and conclude that the standard error of the mean goes from about 1.5 in the 1990s to 2.6 in 2000 and 1.2 × 10^{22} J in 2008. The increased uncertainty about 2000 arises from fewer calibrations and the transition of XBTs to Argo floats. Gouretski et al. (2012) also assess uncertainties for the upper ocean and show a large decrease after 2005. Others included in Fig. 4 are updated from the Hadley Centre (Palmer et al. 2010), Japan Meteorological Agency (JMA; Ishii and Kimoto 2009), the *World Ocean Atlas* (*WOA*; Levitus et al. 2012), and Willis et al. (2008, 2009).

Von Schuckmann and Le Traon (2011) found heat gain based on OHC trends using Argo data of 0.31 W m^{-2} for depths to 700 m averaged over the entire planet for 2005–10 and 0.41 W m^{-2} for depths of 0–2000 m. Hansen et al. (2011) built on these and Lyman et al. (2010) values to estimate the planetary energy imbalance as 0.80 ± 0.20 W m^{-2} for 1993–2008 and 0.58 ± 0.15 W m^{-2} for 2005–10, with estimated 1σ standard error. The nonocean

component rose to about 0.07 W m^{-2} in the 2002–07 period or about 13% of the total. Argo data have also been analyzed by Roemmich and Gilson (2009, 2011) and Willis et al. (2008, 2009). However, Argo data are incomplete in spatial coverage, with gaps over the Indonesian region, the Gulf of Mexico and Caribbean, the Mediterranean Sea, the Sea of Japan, and similar marginal areas, as well as the entire Arctic Ocean.

Unsampled regions in Levitus et al. (2009, 2012) and Gouretski et al. (2012) are assumed to have zero anomalies, and the latter show how resulting sampling errors are problematic in earlier decades. Gregory et al. (2004) showed the sensitivity of results to infilling methods. The assumption of zero anomalies is highly questionable because the climate is changing, and a better approach is to base the first guess on the global or zonal averages of all other observations (Hurrell and Trenberth 1999), as done in some form by Palmer et al. (2007), Lyman and Johnson (2008), and von Schuckmann and Le Traon (2011).

Domingues et al. (2008) and Church et al. (2011) use a reduced set of spatial functions derived from satellite altimeter sea level measurements and thermal expansion observations to analyze sea level and converted a thermosteric component to OHC. Church et al. (2011) estimated an ocean heat uptake of only 0.31 W m^{-2} for 1993–2008, based on a total OHC increase of 79.4 × 10^{21} J made up of 45.9 (0–700 m; 58%), 20.7 (700–3000 m; 26%), and 12.8 (from 3000 m to the bottom; 16%) × 10^{21} J, and this is 91.6% of the total of 86.7 × 10^{21}J when other climate system components are included (0.34 W m^{-2}).

Hence, there are large disparities among analyses (Lyman et al. 2010) in part owing to how data missing in space and time are infilled, although these are reduced after 2005 in the Argo era. Rates of change vary a lot

with the period sampled, but many variations likely are real. All estimates in Lyman et al. (2010) are obtained by statistical interpolation of ocean observations. Model-based data assimilation provides a means to utilize a much richer multivariate database and greatly improves the dynamical consistency and temporal and spatial resolution of the results. Another key issue is the contribution from the deep ocean. Gille (2008) shows how the top 1000 m of ocean has warmed in the Southern Hemisphere. Johnson et al. (2007) and Purkey and Johnson (2010) found the abyssal ocean (below 4000 m) gaining heat at $0.027 \pm 0.009 \, \mathrm{W \, m^{-2}}$ (average for entire globe) in the past 3 decades (95% confidence interval), while from 1000 to 4000 m the rate was $0.068 \pm 0.062 \, \mathrm{W \, m^{-2}}$. Kouketsu et al. (2011) assimilated temperature and salinity data into an ocean general circulation model and found a global increase of $0.8 \times 10^{22} \, \mathrm{J \, decade^{-1}}$ ($0.05 \, \mathrm{W \, m^{-2}}$) for depths exceeding 3000 m for the 1990s–2000s. A recent *WOA* OHC estimate (Levitus et al. 2012) is nominally for 0–2000 m, but in reality covers the depth range to 1750 m and pentadal (5 yr) values are provided so that volcanic eruption and ENSO effects are not resolved. From 1993 to 2011 the rate of increase of OHC at 0–2000 m is about $0.5 \, \mathrm{W \, m^{-2}}$ globally in the *WOA* analysis, and this rate also applies for 2005–10. However, Balmaseda et al. (2013b) show a growing disparity between the OHC changes in the upper 700 and 0–2000 m after 1998. The ORAS4 was produced by combining, every 10 days, the output of an ocean model forced by atmospheric reanalysis fluxes with quality controlled ocean observations. These consist of temperature and salinity (*T* and *S*) profiles from the Hadley Centre's EN3 dataset and altimeter-derived along-track sea level anomalies, while gridded maps of SST are used to adjust the heat fluxes via strong relaxation; see Balmaseda et al. (2013a,b) for details. The ocean model horizontal resolution is approximately 1°, refined meridionally to ⅓° at the equator. There are 42 vertical levels varying smoothly from 10 m at the surface to 300 m at the bottom, with partial cell topography. Bias corrections are applied, and five ensemble members are generated to sample plausible uncertainties in the wind forcing, observation coverage, and the deep ocean. The main estimates of OHC are for the top 700 m of the ocean, and these can be compared, as in Balmaseda et al. (2013a) (Fig. 4). Here it is evident that the ORAS4 estimates are consistent with other estimates overall but there are marked differences in any individual year. Larger rates of increase are apparent in several estimates from the late 1990s to early 2000s with some leveling off after 2005.

An advantage of ORAS4 is that it can also be readily extended to the full-depth ocean and explore the differences between truncating the analysis at 700-m

depth (Fig. 5) (Balmaseda et al. 2013b). For ORAS4 we also make use of the monthly data after 1980 to examine the rates of change of OHC in more detail for the five ensemble members of ORAS4. The overall OHC changes for the top 700 m and total depth (Fig. 5) (Balmaseda et al. 2013b) reveal how the ocean below 700 m has contributed significantly in the past decade to OHC. Here the zero corresponds to the 1958–65 base period. The main contributions below 700 m come from the layer above 2000-m depth.

d. Rates of change of OHC

To evaluate the contributions of changes in OHC to the TOA energy imbalance, it is necessary to differentiate the values to produce rates of change in watts per meter squared. This tests the OHC constructions in ways often not intended by the originators, and how continuity and smoothing in time were ensured make for differences. This process can also be regarded as a high-pass filter as it accentuates the high frequencies and noise. As most OHC values available are annual values, which inherently contain some noise over the arbitrariness of the start and end points and coming and going of observations, it is not surprising when either simple or centered differences result in huge interannual variations. To avoid this, for some analyses the differences are subsequently smoothed with a 1–2–1 binomial filter, which removes the 2-delta fluctuations. The Domingues et al. (2008) values were not annual, but included a 3-yr running mean, and hence these derivatives were not further smoothed. For ORAS4 we exploit the monthly values to examine effects of alternative methodologies for computing the tendencies. Monthly ORAS4 values are valid midmonth, and 12-month differences are taken to remove annual cycle influences.

The collection of results for rates of change of OHC for the top 700 m (Fig. 6) has ORAS4 in the top panel showing that the effects of going from a 12-month running mean to an annual mean mutes many important details, and further detail and amplitude is lost in smoothing. The lower panel, however, reveals that even with smoothing there is a lot of noise, and the unsmoothed rates of most time series are not tenable. ORAS4 is less noisy and has more persistence than the other time series, especially for the ensemble mean. One might hope to see both ENSO and volcanic signals, although neither are well resolved with annual-mean data, as shown by the top panel. A guideline as to the timing of the volcanic signatures is also given in the bottom panel of Fig. 6 for the Mt. Agung (February–March 1963), El Chichón (March–April 1982), and Mt. Pinatubo (June 1991) eruptions with an 18-month window marked.
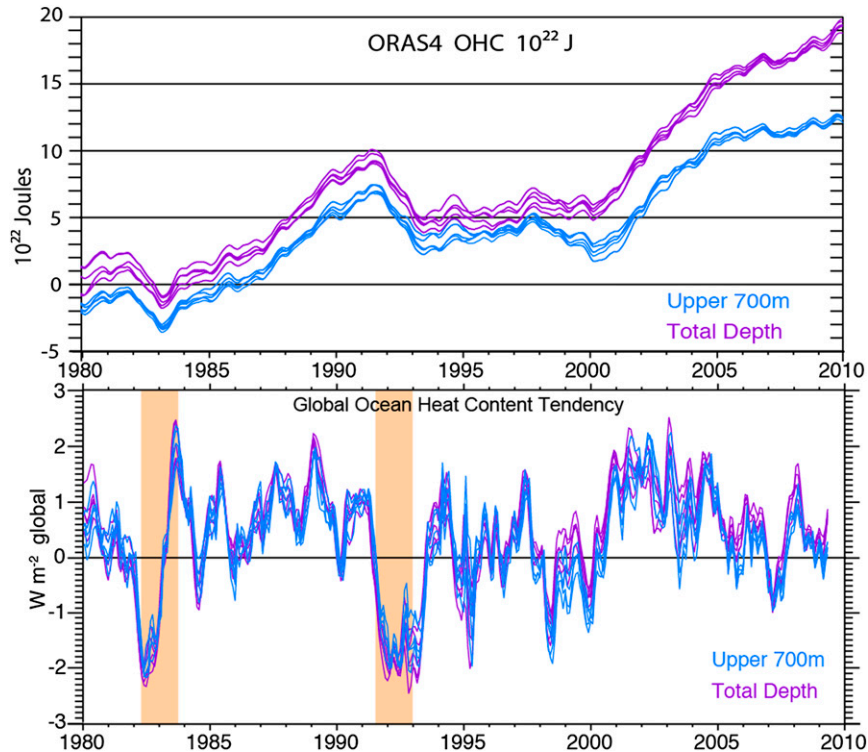
FIG. 5. From ORAS4, for the period after 1980 when the uncertainties are somewhat less, shown are (top) the OHC (10^{22} J) for the upper 700 m and full ocean for all five ensemble members as 12-month running means, the base period (zero) is 1958–65, and (bottom) the corresponding rates of change (for the globe, not global ocean; W m^{-2}). The latter are computed as centered values and with a 12-month running mean. Also shown in the bottom panel in light orange are the 18-month regions following the main volcanic eruptions.

As can be seen from the OHC time series themselves (Fig. 4), there is not much consistency among the rates of change of OHC (Fig. 6). Most values tend to be higher after 1993, reflecting the strong OHC upward trends. Nearly all OHC values suggest a distinct cooling in 1963 with Mt. Agung. Several values are also negative for El Chichón but the timing varies, while JMA and perhaps *WOA* have a modest dip for Mt. Pinatubo, as was also noted by Church et al. (2005). Magnitudes are less than 1 W m^{-2}, which is to be expected given the temporal resolution and smoothing. It is evident that annual-mean data are insufficient for sorting out interannual variability. Figure 6 helps put the discussion of the literature (section 2c) in context and cautions on choosing a single value for rates of change. The largest uncertainty in the decadal OHC rate of change happens between 1993 and 2005 in the transition from XBTs to Argo.

The lower panel of Fig. 5 shows the ORAS4 rates of change computed for the full globe for both 0–700 m and the full-depth of the ocean. Here the rates are computed from a 12-month running mean of the centered differences. Accordingly, there is leakage from a step function

change such as a volcanic event, and the sharp drop that apparently occurs beginning late 1981 in fact is a consequence of a sharp drop in March 1982. Nevertheless, the abrupt coolings in 1982 and 1992 associated with the volcanic eruptions are clearly evident in ORAS4 in Fig. 5. Here the drop following Pinatubo of 5×10^{22} J is larger than the 3×10^{22} J found by Church et al. (2005). The rates of change for the two layers are quite similar until the early 1990s, but they diverge after 1998 with the total depth ocean values higher by 0.21 W m^{-2} on average for the 2000s. While information about El Chichón in ORAS4 comes mainly from the subsurface ocean measurements, SST plays a more prominent role for Pinatubo (see Fig. S05 in the supplementary material of Balmaseda et al. 2013b).

When the five-member ensemble results from ORAS4 are compared for the full ocean (Fig. 7) with values expected from CCSM4 in Fig. 1, however, the very distinctive volcanic signatures are seen to have the right order of magnitude and duration. In fact the El Chichón OHC signature precedes that from CCSM4 and this, as shown in Fig. 3, is built into the profile of the delayed
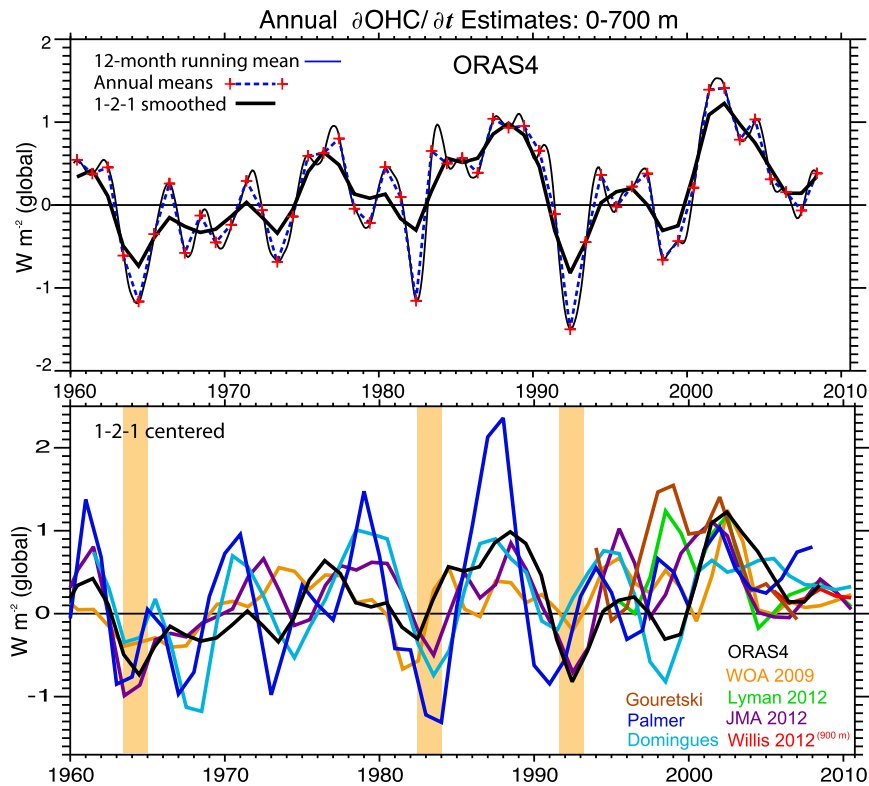
FIG. 6. Rates of change of OHC 0–700 m (global; W m^{-2}) for the analyses as given in the key. (top) The ORAS4 analyses are used to illustrate the effects of subsampling and smoothing. Shown are the ensemble-mean 12-month running-mean values, the equivalent annual-mean calendar year values as red crosses (dashed line), and the 1–2–1 smoothed values. (bottom) Annual OHC values are center differenced to get rates and then 1–2–1 smoothed. The light orange bars in the bottom panel give the times of the three main volcanic events.

forcing imposed in CCSM4, whereby the peak radiative forcing is in September 1982, some 6 months after the peak loss of radiation measured in Hawaii. However, ENSO (see below) may also be a factor. Nevertheless, there is a distinctive volcanic signal in OHC whose rate of change is quantitatively compatible with that expected from the inferred TOA energy imbalance. It is, however, essential to include the layers below 700 m in this calculation, and it is necessary to have subannual resolution.

At other times, the agreement between the ORAS4 and CCSM4 TOA radiation (Fig. 7) is reasonable. Although quite a few values are outside the one standard deviation CCSM4 values, most are within two standard deviations. From 1994 to 2000 values in ORAS4 are well below CCSM4 values, but they jump to higher than CCSM4 values from 2001 to 2005. A notable departure is the 1997/98 El Niño, which took enormous amounts of heat out of the tropical Pacific Ocean (Balmaseda et al. 2013b). El Niño events (marked on Fig. 7) can be seen as often creating such relative dips, sometimes with a delay

in recovery. It is therefore worthwhile exploring the ENSO variability further.

e. ENSO events

The El Niño events, as given by the National Oceanic and Atmospheric Administration (NOAA) oceanic Niño index (ONI), are marked on Fig. 7 by orange bands denoting the duration of each event, based on a threshold of ±0.5°C for the ONI [3-month running mean of SST anomalies in the Niño-3.4 region (5°N–5°S, 120–170°W), calculated with respect to the 1971–2000 base period]. El Niño events occurred concurrently with volcanic eruptions during 1) July 1963–January 1964 versus Mt. Agung eruption February–March 1963; 2) May 1982–June 1983 versus El Chichón eruption March–April 1982; and 3) May 1991–July 1992 versus Mt. Pinatubo eruption June 1991. During the course of an El Niño event, the initial redistribution of ocean heat turns to an ocean loss as the atmosphere warms (Trenberth et al. 2002), and this can often be seen in the change in OHC (Fig. 7).
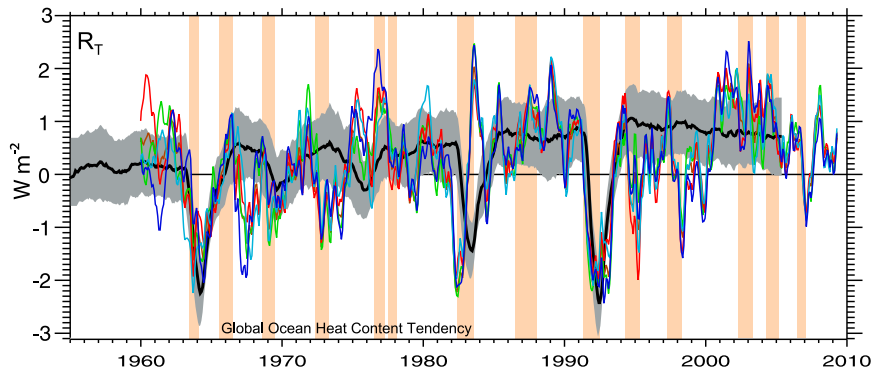
FIG. 7. Rates of change for each of the five member ensemble members of ORAS4 OHC to the bottom of the ocean (global; $W\,m^{-2}$). In addition, the ensemble mean and monthly standard deviation of CCSM4 R_T (from Fig. 1) is given. El Niño events are marked by the light orange bars, as defined by the ONI index of NOAA.

Hence, we have further examined the evolution of El Niño events throughout the ORAS4 record (Fig. 8). The expected evolution of OHC in ENSO events is largely missing prior to 1992. Most of the tropical Pacific moored array was established throughout 1992/93, and space-based altimetry was also established in late 1992. Accordingly, the observing system was very likely not adequate to properly specify the tropical Pacific OHC in ORAS4 analyses for earlier events. We have therefore focused on the events after that time in the form of composites of their evolution.

A listing of El Niño events, as defined by the ONI and given here by the leading letters of the months after 1992, includes from April–June (AMJ) 1991 to June–August (JJA) 1992 (14 months); from AMJ 1994 to February–April (FMA) 1995 (10 months); from AMJ 1997 to AMJ 1998 (12 months); from AMJ 2002 to FMA 2003 (10 months); from May–July (MJJ) 2004 to January–March (JFM) 2005 (8 months); and from July–September (JAS) 2006 to December–February (DJF) 2007 (4 months). The amplitude of the ONI variations and the composite mean (Fig. 8, top) is centered with the maximum at time zero, but the amplitudes and durations vary enormously. In the lower two panels the individual events are given for the rates of change of OHC along with the composite mean and standard deviation about that mean for the global ocean (middle) and tropical Pacific Ocean (30°S–30°N, 125°E–100°W) (bottom). These reveal a drop in rates of change of OHC from generally positive 2 or 3 months before the peak event to negative 4 months after the event in the tropical Pacific and a more sustained cooling for the global ocean for up to and even beyond a year after the peak event. The 1997/98 event is exceptional both in terms of the ONI and the magnitude of the change in the Pacific. The 2005 event is less consistent but was also the weakest event.

Clearly the tendency for a reduction in OHC during the course of an El Niño event and the coincidence of these events with the volcanic eruptions confounds the simple interpretation of both, and there are too few events to allow this to be reliably sorted out. While it is possible that there is some spurious variability present in ORAS4, perhaps associated with observing system changes and sampling, it is equally likely that the level of natural variability in CCSM4 may be slightly underestimated on decadal time scales.

3. Changes in energy balance over the past decade: CERES versus OHC

After March 2000, CERES estimates of the TOA radiative imbalance are available, and although there is uncertainty in their absolute calibration, their temporal stability makes them useful to compare with OHC changes over time. The CERES observational record (Fig. 9) reveals that in 2008/09 there was extra TOA energy absorption (Wong et al. 2009). The Niño-3.4 SST index (Fig. 9) reveals strong La Niña conditions near this time, indicating lower than normal SSTs in the tropical Pacific. Temperatures were below normal globally, and January 2008 was the coldest month relative to normal this century. This led to lower OLR, but was accompanied by an increase in ASR, as clouds decreased in amount, leaving a pronounced net heating ($>1.5\,W\,m^{-2}$; cf. Loeb et al. 2009) of the planet for about a year during 2008/09 (Fig. 9). Moreover, as shown above, ocean temperature measurements for 0–700 m from 2005 to 2008 suggested a substantial slowing of the increase in global OHC (Lyman et al. 2010; Levitus et al. 2009) precisely during the time when CERES estimates depict an increase in the planetary imbalance, compounding the disparity. So where did the heat go?
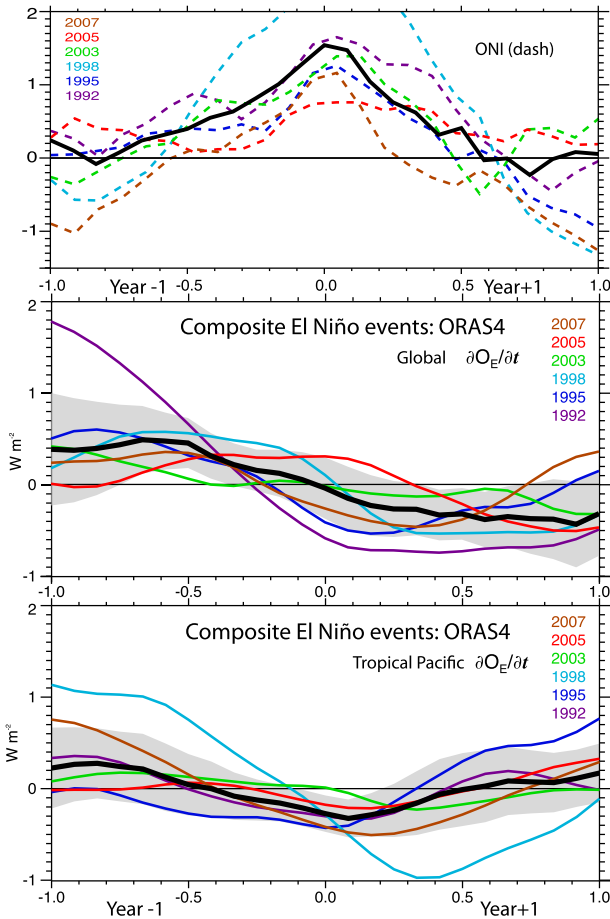
FIG. 9. Net radiation from the TOA from CERES [Energy Balanced and Filled (EBAF) Ed2.6r; http://ceres.larc.nasa.gov/products.php?product=EBAF]. The ASR (red) and OLR (blue) are given on the right axis and R_T (ASR − OLR; black) is given on the left axis (W m^{-2}; note the change in scale). For ASR, OLR, and R_T, the ±1 standard deviation range is given in light red, blue, and gray. Also shown is the Niño-3.4 SST index (green; right axis, °C). The decadal low-pass filter is a 13-term filter used in Trenberth et al. (2007), making it similar to a 12-month running mean.

FIG. 8. (top) Composite mean of six events after 1992 and five ensembles for the El Niño events as noted for 1 yr prior to and 1 yr after the peak in the El Niño indices for ONI. The individual rates of change of OHC from ORAS4 for the (middle) global ocean and (bottom) tropical Pacific Ocean along with the composite mean (black) are shown, with ±1 standard deviation about the composite mean in light gray. In the middle and bottom panels, the units are normalized to the global area, and so the actual values should be increased by factors of 1.42 and 5.00 to get watts per meter squared (W m^{-2}) for the global ocean and tropical Pacific, respectively.

Some heat has gone into the record-breaking loss of Arctic sea ice, and some has undoubtedly contributed to unprecedented melting of Greenland (van den Broeke et al. 2009) and Antarctica (Chen et al. 2009), but these anomalies are unable to account for much of the measured TOA energy imbalance. This apparent discrepancy gave rise to the concept of missing energy (Trenberth and Fasullo 2010). Revisions have occurred in both the CERES and OHC datasets, and the changes to CERES (Trenberth and Fasullo 2011) have reduced the discrepancy by about 15%.

Another interpretation is that there is no missing energy because the error bars were not adequately accounted for, and they are quite big (Trenberth and Fasullo 2011),
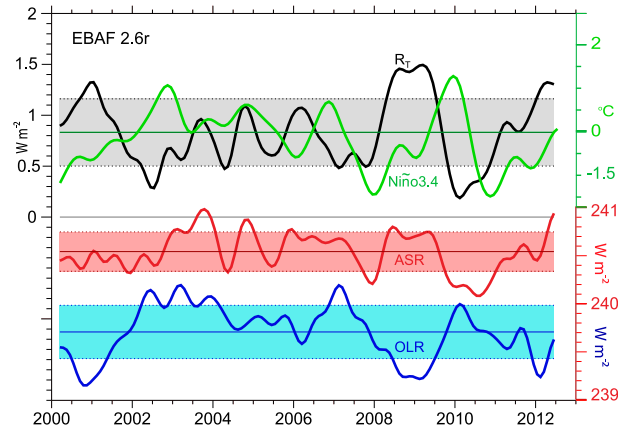
especially for OHC changes from one year to the next (see above). Loeb et al. (2012) claim that this is the case, yet the error bars in their analysis are somewhat large owing to conflation of the systematic with random error. As noted, the systematic bias is uncertain but CERES drift over the period is relatively small (<0.3 W m^{-2} decade^{-1}; Loeb et al. 2009). Loeb et al. (2012) assigned a one standard deviation uncertainty in CERES net TOA flux for individual years as 0.31 W m^{-2}, determined by adding in quadrature the mean net TOA flux uncertainty of 0.2 W m^{-2} and a random component from the root-mean-square difference between CERES *Terra* and *Aqua* global annual-mean net TOA flux values that amounts to a standard deviation of 0.24 W m^{-2}. It is this latter value that is more appropriate for use in examining year-to-year variations. Further errors may arise from the absence of short-term weather sampling in CERES.

Figure 10 shows an alternative error analysis with the same three OHC datasets used by Loeb et al. (2012) (plus ORAS4, which is discussed below) for the top 700 m of the ocean. OHC rates of change were computed using the centered differences and a 1–2–1 smoothing [versus a simple one-sided difference in Loeb et al. (2012)], and the error bars are based on Lyman et al. (2010), modified to account for the smoothing. All values correspond to middle of the year estimates, but are offset slightly for plotting purposes. The 12-month running-mean OHC tendencies from ORAS4 for each ensemble member are also given, along with new results
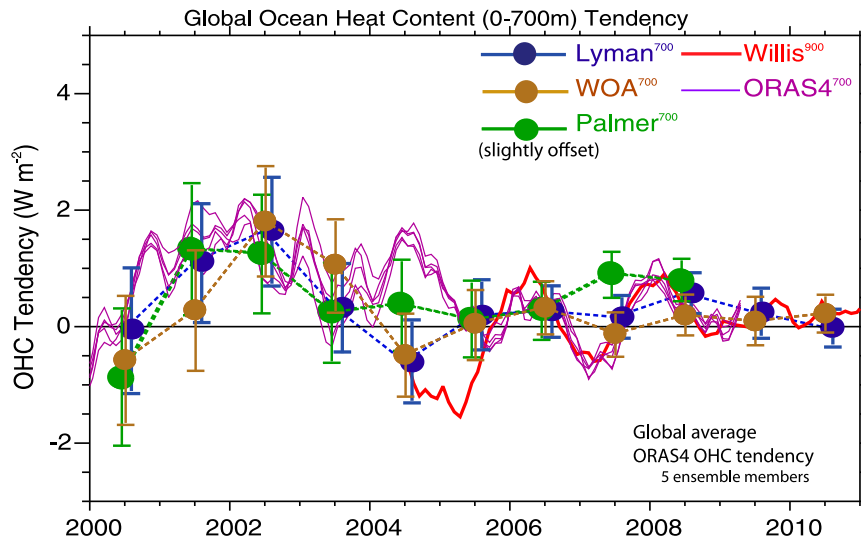
FIG. 10. Comparison of rates of change of global-averaged OHC ($W\,m^{-2}$) down to 700-m depth (900 m for Willis) from the *WOA* (Levitus et al. 2012), Hadley Centre (Palmer), and NOAA Pacific Marine Environmental Laboratory (Lyman) and 1σ standard error uncertainty bounds (vertical lines) based on Lyman et al. (2010) and modified to account for the smoothing, slightly offset from one another and computed as centered differences between annual means with 1–2–1 smoothing, except for ORAS4 and Willis, which are 12-month running means. ORAS4 includes all five ensemble members.

using Argo data from Willis et al. (2008, 2009). The Argo data seem astray in 2004/05 when the numbers were spinning up (see also Fig. 11). Otherwise there is reasonable agreement.

Rather than compare these directly with CERES, it is important to include the layer below 700 m, as in Fig. 11. Here the full-depth ORAS4 is included along with estimates from *WOA* down to 2000 m and Argo data from Roemmich and Gilson (2009, 2011) and von Schuckmann and Le Traon (2011) (updated in all cases). Error bars for the latter for OHC are about $\pm 1 \times 10^{22}$ J, which converts to an error bar in rates of change on annual time scales of about $\pm 0.36\,W\,m^{-2}$. Figure 11 also shows the estimated CERES net TOA imbalance and associated uncertainty, while accounting for a drift in the CERES estimates ($0.3\,W\,m^{-2}\,decade^{-1}$) (shaded and dotted red lines). The CERES data are plotted as 12-month running means for consistency, but calibrated to an energy imbalance overall of $0.8\,W\,m^{-2}$ (consistent with the overall energy imbalance from ORAS4 for the 2000s, extended to 2011) that could be adjusted up or down somewhat. They are lower than the OHC values for 2000–04 (Figs. 10, 11), but higher in 2008/09 when there remains missing energy that is outside of the error bars. In 2001/02 there are discrepancies on the low side for CERES, while in 2007 and 2009 the discrepancies are on the high side. In 2009, the discrepancy is particularly large relative to OHC uncertainty and exceeds 2σ in

magnitude for both the Lyman and Palmer estimates (Fig. 10) and *WOA*, Argo, and ORAS4 (Fig. 11), thus exceeding the 5% significance level. Once again the Argo estimates prior to 2005 seem highly suspect. The von Schuckmann estimate does not (yet) include allowance for the top 10 m of the ocean (to be estimated using SSTs) or 1500–2000 m, but these are expected shortly.

ORAS4 (Fig. 11) supports the other OHC analyses that there is strong warming of order $1\,W\,m^{-2}$ in the early 2000s and somewhat less in recent years. All estimates support the dip (cooling) in 2007, seen as much weaker by CERES, and they fail to adequately resolve the strong heating in 2008/09 reported by CERES. Varying the assumptions of the mean imbalance between 0 and $1\,W\,m^{-2}$ is unable to achieve closure in many years, especially 2002, 2005, 2007, and 2009, depending on the value of the imbalance chosen. In other words, it is possible to fit the CERES values within bounds to match some but not all estimates of OHC change during its period of concurrent coverage, and during many intervals the agreement between ORAS4 and CERES is not strong.

The inability to achieve closure in the late 2000s under reasonable assumptions of the TOA imbalance (0.5–$1.0\,W\,m^{-2}$) may be attributable to the remaining errors in either CERES or in OHC (e.g., related to biases in sampling, especially in the Arctic Ocean, which is missing
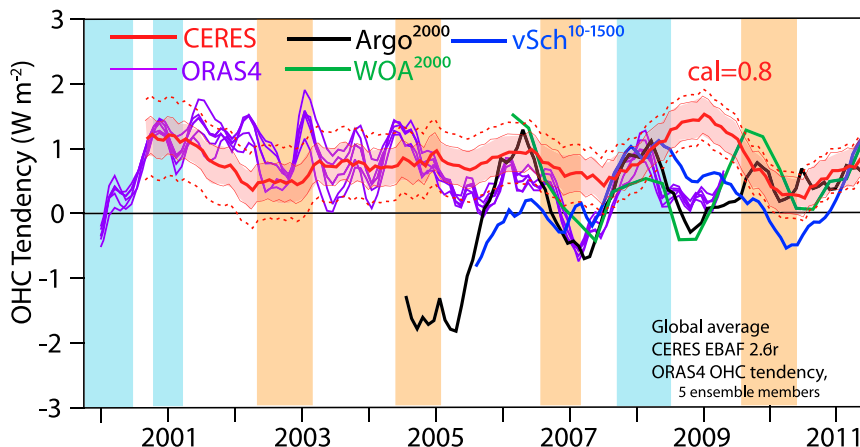
FIG. 11. The 12-month running-mean tendency from ORAS4 full-depth ocean OHC tendencies are given in purple for all five ensemble members along with updated estimates from the *WOA* (Levitus et al. 2012) and Argo as analyzed by Roemmich and Gilson (2009, 2011) and von Schuckmann and Le Traon (2011). Also shown is an estimate of the TOA imbalance based on CERES estimates (red solid lines) with 1σ standard error uncertainty bounds (pink shading) for random errors based on Loeb et al. (2012) and drift (dotted lines) under an assumption of net radiative imbalance at TOA of $0.8\,\mathrm{W\,m^{-2}}$. Vertical light orange bars indicate El Niño events and light blue bars La Niña events as given by the ONI from NOAA.

in all Argo-based analyses) and suggests that some missing energy remains. Yet if the error bars are so big that there is no mismatch, as suggested by Loeb et al. (2012), then the values are not useful for these purposes because they fail to provide a constraint on interannual or longer-term variations in energy in the climate system. In either case, there is a clear need for further improvement in observational and analytical capabilities.

Further, it was postulated that undersampling of the ocean, especially below 700 m and in the deep ocean, may account for the main discrepancy, as it is manifested at only certain times (when La Niña is present). Palmer et al. (2011) show how OHC with depth relates to SST and the importance of the deep ocean in properly assessing the energy imbalance in their model. Meehl et al. (2011, 2013) and Trenberth and Fasullo (2011) explored the extent to which this kind of behavior occurs in CCSM4. Several runs with the model under future emissions scenarios where the radiative imbalance is known exactly and a distinct energy imbalance at TOA was occurring nonetheless featured several stases in surface temperatures for more than a decade. Examination of the energy flows during such intervals for all ensemble members reveals a consistent picture. The net radiation at the TOA (R_T) was on the order of $1\,\mathrm{W\,m^{-2}}$ into the climate system, yet there was a stasis in warming at the surface. Examination of the changes in OHC showed clearly that this was the main sink. Indeed, the full-depth OHC continued relentlessly upward with no hesitation at all. Hence, the missing heat was being

deposited mainly below 700-m depth. Moreover, the stasis periods corresponded to La Niña or negative Pacific decadal oscillation conditions. The ORAS4 data seem to confirm this picture, as recently documented (Trenberth and Fasullo 2013). Since 2005, the rate of increase in OHC above 700 m has slowed considerably, but from 0 to 2000 m, the OHC has continued to increase (Figs. 4, 5), and this is also found in other analyses that have recently been extended (Levitus et al. 2012; von Schuckmann and Le Traon 2011), albeit at various rates.

4. Conclusions

From the estimates discussed here, it is clear that the net energy imbalance at TOA varies naturally in response to weather and climate variations, the most distinctive of which is ENSO. It also varies with the sunspot cycle. Moreover, the net TOA energy flux is profoundly influenced by volcanic eruptions (not new) and almost simultaneously, but with some blurring, so too is OHC. All of these influences occur superposed on the climate change signals associated with changes in atmospheric composition.

While previous estimates of OHC changes over time have revealed an overall upward trend, their agreement with regard to interannual and even interdecadal variability has been lacking. An obvious key issue is the extent to which the main large climate signals associated with volcanic eruptions and ENSO are clearly evident in the OHC tendencies. ORAS4 has clear volcanic signals

following Mt. Agung (1963), El Chichón (1982), and Pinatubo (1991) eruptions, but they are not as clear in other OHC reconstructions, in part because of inadequate temporal resolution. Differences further highlight the remaining issues of adequately dealing with missing data in space and time and how OHC is mapped. The ORAS4 product appears to be a substantial advance in these respects. ORAS4 also has some distinctive ENSO signals after 1992 when the ocean observing system in the tropical Pacific improved markedly, consistent with earlier expectations and the more detailed recent analysis of Roemmich and Gilson (2011). The ability of ORAS4 to adequately resolve such signals is a testament to the reanalysis procedure, offering a viable path forward for improved OHC estimation. However, the continuity of reanalyses is still vulnerable to the changing observing system.

After the effects of Mt. Pinatubo died away in about 1994, several estimates (Trenberth et al. 2009; Hansen et al. 2011; Lyman et al. 2010; Balmaseda et al. 2013b) support the view that the energy imbalance was order $1.0 \, \mathrm{W \, m^{-2}}$ from 2000 through 2004. From 2005 to 2010, the quiet sun reduced the energy imbalance by 0.1–$0.15 \, \mathrm{W \, m^{-2}}$ (Fig. 2) and there was a noticeable slowing of the increase in OHC above 700-m depth, but not as much as for the full-depth OHC, that has led to reduced estimates of the overall energy imbalance to 0.3–$0.8 \, \mathrm{W \, m^{-2}}$ in the latter part of the decade. Assessments such as those by Hansen et al. (2011) and Church et al. (2011) suggest that the TOA imbalance has slowed, in contradiction to the CERES measurements. Here we have used ORAS4 to include the contributions to total OHC from the deeper ocean. The analysis has reinforced and refined estimates from Levitus et al. (2012) that the contribution is significant. For the 2000s, with $0.07 \, \mathrm{W \, m^{-2}}$ for other components, the total energy imbalance implied by ORAS4 is $0.91 \pm 0.10 \, \mathrm{W \, m^{-2}}$; this is also about the value preferred by CCSM4 (Fig. 1).

Yet, closure of the observed energy budget over the past 5 years remains largely elusive for interannual variations (Trenberth 2009; Trenberth and Fasullo 2010). While some of the previously missing energy is accounted for, substantial discrepancies between OHC and CERES at interannual time scales persist and are especially prominent during 2008/09. Thus, state-of-the-art observations and basic analysis are unable to completely account for recent energy variability at interannual time scales, since they provide either an incoherent narrative or imply error bars too large to make the products useful. Both TOA radiation and OHC datasets need to be improved further. A vital need exists for OHC datasets of at least seasonal resolution, with care taken to reduce spurious noise, if real variations in nature are to be adequately understood.

REFERENCES

Abraham, J. P., and Coauthors, 2013: A review of global ocean temperature observations: Implications for ocean heat content estimates and climate change. *Rev. Geophys.,* **51,** 450–483, doi:10.1002/rog.20022.

Ammann, C. M., G. A. Meehl, W. M. Washington, and C. Zender, 2003: A monthly and latitudinally varying volcanic forcing dataset in simulations of 20th century climate. *Geophys. Res. Lett.,* **30,** 1657, doi:10.1029/2003GL016875.

Balmaseda, M. A., K. Mogensen, and A. T. Weaver, 2013a: Evaluation of the ECMWF Ocean Reanalysis ORAS4. *Quart. J. Roy. Meteor. Soc.,* **139,** 1132–1161, doi:10.1002/qj.2063.

——, K. E. Trenberth, and E. Källén, 2013b: Distinctive climate signals in reanalysis of global ocean heat content. *Geophys. Res. Lett.,* **40,** 1754–1759, doi:10.1002/grl.50382.

Bindoff, N. L., and Coauthors, 2007: Observations: Oceanic climate change and sea level. *Climate Change 2007: The Physical Science Basis,* S. Solomon et al., Eds., Cambridge University Press, 385–432.

Chen, J. L., C. R. Wilson, D. Blankenship, and B. D. Tapley, 2009: Accelerated Antarctic ice loss from satellite gravity measurements. *Nat. Geosci.,* **2,** 859–862, doi:10.1038/ngeo694.

Church, J. A., N. J. White, and J. M. Arblaster, 2005: Significant decadal-scale impact of volcanic eruptions on sea level and ocean heat content. *Nature,* **438,** 74–77, doi:10.1038/nature04237.

——, and Coauthors, 2011: Revisiting the Earth's sea-level and energy budgets from 1961 to 2008. *Geophys. Res. Lett.,* **38,** L18601, doi:10.1029/2011GL048794.

Deluisi, J., E. G. Dutton, K. L. Coulson, T. E. DeFoor, and B. G. Mendonca, 1983: On some radiative features of the El Chichón volcanic stratospheric dust cloud and a cloud of unknown origin observed at Mauna Loa. *J. Geophys. Res.,* **88,** 6769–6772, doi:10.1029/JC088iC11p06769.

Domingues, C. M., J. A. Church, N. J. White, P. J. Gleckler, S. E. Wijffels, P. M. Barker, and J. R. Dunn, 2008: Improved estimates of upper-ocean warming and multi-decadal sea-level rise. *Nature,* **453,** 1090–1093, doi:10.1038/nature07080.

Dutton, E. G., and B. A. Bodhaine, 2001: Solar irradiance anomalies caused by clear-sky transmission variations above Mauna Loa: 1958–99. *J. Climate,* **14,** 3255–3262, doi:10.1175/1520-0442(2001)014<3255:SIACBC>2.0.CO;2.

Fasullo, J. T., and K. E. Trenberth, 2008a: The annual cycle of the energy budget. Part I: Global mean and land–ocean exchanges. *J. Climate,* **21,** 2297–2312, doi:10.1175/2007JCLI1935.1.

——, and ——, 2008b: The annual cycle of the energy budget. Part II: Meridional structures and poleward transports. *J. Climate,* **21,** 2313–2325, doi:10.1175/2007JCLI1936.1.

Gent, P. R., and Coauthors, 2011: The Community Climate System Model version 4. *J. Climate,* **24,** 4973–4991, doi:10.1175/2011JCLI4083.1.

Gille, S. T., 2008: Decadal-scale temperature trends in the southern hemisphere ocean. *J. Climate,* **21,** 4749–4765, doi:10.1175/2008JCLI2131.1.

Gouretski, V., and F. Reseghetti, 2010: On depth and temperature biases in bathythermograph data: Development of a new correction scheme based on analysis of a global ocean database. *Deep-Sea Res. I,* **57,** 812–833, doi:10.1016/j.dsr.2010.03.011.

——, J. Kennedy, T. Boyer, and A. Köhl, 2012: Consistent near-surface ocean warming since 1900 in two largely independent observing networks. *Geophys. Res. Lett.,* **39,** L19606, doi:10.1029/2012GL052975.

Gregory, J. M., H. T. Banks, P. A. Stott, J. A. Lowe, and M. D. Palmer, 2004: Simulated and observed decadal variability in ocean heat content. *Geophys. Res. Lett.,* **31,** L15312, doi:10.1029/2004GL020258.

Hansen, J., M. Sato, P. Kharecha, and K. von Schuckmann, 2011: Earth's energy imbalance and implications. *Atmos. Chem. Phys.,* **11,** 13 421–13 449, doi:10.5194/acp-11-13421-2011.

Hurrell, J. W., and K. E. Trenberth, 1999: Global sea surface temperature analyses: Multiple problems and their implications for climate analysis, modeling, and reanalysis. *Bull. Amer. Meteor. Soc.,* **80,** 2661–2678, doi:10.1175/1520-0477(1999)080<2661:GSSTAM>2.0.CO;2.

Ishii, M., and M. Kimoto, 2009: Reevaluation of historical ocean heat content variations with time-varying XBT and MBT depth bias corrections. *J. Oceanogr.,* **65,** 287–299, doi:10.1007/s10872-009-0027-7.

Johnson, G. C., S. Mecking, B. M. Sloyan, and S. E. Wijffels, 2007: Recent bottom water warming in the Pacific Ocean. *J. Climate,* **20,** 5365–5375, doi:10.1175/2007JCLI1879.1.

——, J. M. Lyman, J. K. Willis, S. Levitus, T. Boyer, J. Antonov, and S. A. Good, 2012: Global oceans: Ocean heat content [in "State of the Climate in 2011"]. *Bull. Amer. Meteor. Soc.,* **93,** S62–S65, doi:10.1175/2012BAMSStateoftheClimate.1.

Kouketsu, S., and Coauthors, 2011: Deep ocean heat content changes estimated from observation and reanalysis product and their influence on sea level change. *J. Geophys. Res.,* **116,** C03012, doi:10.1029/2010JC006464.

Levitus, S., J. I. Antonov, T. P. Boyer, R. A. Locarnini, H. E. Garcia, and A. V. Mishonov, 2009: Global ocean heat content 1955–2008 in light of recently revealed instrumentation problems. *Geophys. Res. Lett.,* **36,** L07608, doi:10.1029/2008GL037155.

——, and Coauthors, 2012: World ocean heat content and thermosteric sea level change (0–2000 m), 1955–2010. *Geophys. Res. Lett.,* **39,** L10603, doi:10.1029/2012GL051106.

Loeb, N. G., B. A. Wielicki, D. R. Doelling, G. L. Smith, D. F. Keyes, S. Kato, N. Manalo-Smith, and T. Wong, 2009: Towards optimal closure of the Earth's top-of-atmosphere radiation budget. *J. Climate,* **22,** 748–766, doi:10.1175/2008JCLI2637.1.

——, J. M. Lyman, G. C. Johnson, R. P. Allan, D. R. Doelling, T. Wong, B. J. Soden, and G. L. Stephens, 2012: Observed changes in top-of-the-atmosphere radiation and upper-ocean heating consistent within uncertainty. *Nat. Geosci.,* **5,** 110–113, doi:10.1038/NGEO1375.

Lyman, J. M., and G. C. Johnson, 2008: Estimating global upper ocean heat content despite irregular sampling. *J. Climate,* **21,** 5629–5641, doi:10.1175/2008JCLI2259.1.

——, S. A. Good, V. V. Gouretski, M. Ishii, G. C. Johnson, M. D. Palmer, D. M. Smith, and J. K. Willis, 2010: Robust warming of the global upper ocean. *Nature,* **465,** 334–337, doi:10.1038/nature09043.

Meehl, G. A., J. M. Arblaster, J. T. Fasullo, A. Hu, and K. E. Trenberth, 2011: Model-based evidence of deep-ocean heat uptake during surface-temperature hiatus periods. *Nat. Climate Change,* **1,** 360–364, doi:10.1038/nclimate1229.

——, A. Hu, J. Arblaster, J. T. Fasullo, and K. E. Trenberth, 2013: Externally forced and internally generated decadal climate variability in the Pacific. *J. Climate,* **26,** 7298–7310, doi:10.1175/JCLI-D-12-00548.1.

Murphy, D. M., S. Solomon, R. W. Portmann, K. H. Rosenlof, P. M. Forster, and T. Wong, 2009: An observationally based energy balance for the Earth since 1950. *J. Geophys. Res.,* **114,** D17107, doi:10.1029/2009JD012105.

Palmer, M. D., K. Haines, S. F. B. Tett, and T. J. Ansell, 2007: Isolating the signal of ocean global warming. *Geophys. Res. Lett.,* **34,** L23610, doi:10.1029/2007GL031712.

——, and Coauthors, 2010: Future observations for monitoring global ocean heat content. *Proc. OceanObs '09: Sustained Ocean Observations and Information for Society Conf.,* Vol. 2, ESA Publication WPP-306, Venice, Italy, ESA, doi:10.5270/OceanObs09.cwp.68.

——, D. J. McNeall, and N. J. Dunstone, 2011: Importance of the deep ocean for estimating decadal changes in Earth's radiation. *Geophys. Res. Lett.,* **38,** L13707, doi:10.1029/2011GL047835.

Purkey, S. G., and G. C. Johnson, 2010: Warming of global abyssal and deep southern ocean between the 1990s and 2000s: Contributions to global heat and sea level rise budgets. *J. Climate,* **23,** 6336–6351, doi:10.1175/2010JCLI3682.1.

Roemmich, D., and J. Gilson, 2009: The 2004–2008 mean and annual cycle of temperature, salinity, and steric height in the global ocean from the Argo program. *Prog. Oceanogr.,* **82,** 81–100, doi:10.1016/j.pocean.2009.03.004.

——, and ——, 2011: The global ocean imprint from ENSO. *Geophys. Res. Lett.,* **38,** L13606, doi:10.1029/2011GL047992.

Solomon, S., D. Qin, M. Manning, Z. Chen, M. Marquis, K. Averyt, M. Tignor, and H. L. Miller Jr., Eds., 2007: *Climate Change 2007: The Physical Science Basis.* Cambridge University Press, 996 pp.

——, K. H. Rosenlof, R. W. Portmann, J. S. Daniel, S. M. Davis, T. J. Sanford, and G.-K. Plattner, 2010: Contributions of stratospheric water vapor to decadal changes in the rate of global warming. *Science,* **327,** 1219–1223, doi:10.1126/science.1182488.

——, J. S. Daniel, R. R. Neely III, J.-P. Vernier, E. G. Dutton, and L. W. Thomason, 2011: The persistently variable "background" stratospheric aerosol layer and global climate change. *Science,* **333,** 866–870, doi:10.1126/science.1206027.

Trenberth, K. E., 2009: An imperative for adapting to climate change: Tracking Earth's global energy. *Curr. Opin. Environ. Sustainability,* **1,** 19–27, doi:10.1016/j.cosust.2009.06.001.

——, and A. Dai, 2007: Effects of Mount Pinatubo volcanic eruption on the hydrological cycle as an analog of geoengineering. *Geophys. Res. Lett.,* **34,** L15702, doi:10.1029/2007GL030524.

——, and J. T. Fasullo, 2008: An observational estimate of ocean energy divergence. *J. Phys. Oceanogr.,* **38,** 984–999, doi:10.1175/2007JPO3833.1.

——, and ——, 2010: Tracking Earth's energy. *Science,* **328,** 316–317, doi:10.1126/science.1187272.

——, and ——, 2011: Tracking Earth's energy: From El Niño to global warming. *Surv. Geophys.,* **33,** 413–426, doi:10.1007/s10712-011-9150-2.

——, and ——, 2013: An apparent hiatus in global warming? *Earth's Future,* **1,** 19–32, doi:10.1002/2013EF000165.

——, J. M. Caron, D. P. Stepaniak, and S. Worley, 2002: The evolution of ENSO and global atmospheric surface temperatures. *J. Geophys. Res.,* **107** (D8), doi:10.1029/2000JD000298.

——, and Coauthors, 2007: Observations: Surface and atmospheric climate change. *Climate Change 2007: The Physical Science Basis,* S. Solomon et al., Eds., Cambridge University Press, 235–336.

——, J. T. Fasullo, and J. Kiehl, 2009: Earth's global energy budget. *Bull. Amer. Meteor. Soc.,* **90,** 311–323, doi:10.1175/2008BAMS2634.1.

van den Broeke, M., and Coauthors, 2009: Partitioning recent Greenland mass loss. *Science,* **326,** 984–986, doi:10.1126/science.1178176.

Vernier, J.-P., and Coauthors, 2011: Major influence of tropical volcanic eruptions on the stratospheric aerosol layer during the last decade. *Geophys. Res. Lett.,* **38,** L12807, doi:10.1029/2011GL047563.

von Schuckmann, K., and P.-Y. Le Traon, 2011: How well can we derive global ocean indicators from Argo data? *Ocean Sci.,* **7,** 783–791, doi:10.5194/os-7-783-2011.

Willis, J. K., D. P. Chambers, and R. S. Nerem, 2008: Assessing the globally averaged sea level budget on seasonal to interannual timescales. *J. Geophys. Res.,* **113,** C06015, doi:10.1029/2007JC004517.

——, J. M. Lyman, G. C. Johnson, and J. Gilson, 2009: In situ data biases and recent ocean heat content variability. *J. Atmos. Oceanic Technol.,* **26,** 846–852, doi:10.1175/2008JTECHO608.1.

Wong, T., P. W. Stackhouse Jr., D. P. Kratz, and A. C. Wilber, 2009: Earth radiation budget at top-of-atmosphere [in "State of the Climate in 2008"]. *Bull. Amer. Meteor. Soc.,* **90,** S33–S34, doi:10.1175/BAMS-90-8-StateoftheClimate.

Xue, Y., and Coauthors, 2012: A comparative analysis of upper-ocean heat content variability from an ensemble of operational ocean reanalyses. *J. Climate,* **25,** 6905–6929, doi:10.1175/JCLI-D-11-00542.1.